HYPK promotes the activity of the N-alpha acetyltransferase A complex to determine proteostasis of nonAc-X 2 /N-degron-containing proteins

Pavlína Miklánková, Eric Linster, Jean-Baptiste Boyer, Jonas Weidenhausen, Johannes Mueller, Laura Armbruster, Karine Lapouge, Carolina de la Torre, Willy Bienvenut, Carsten Sticht, et al.

PLANT SCIENCES

HYPK promotes the activity of the N^{α}-acetyltransferase A complex to determine proteostasis of nonAc-X^2/N-degron–containing proteins

Pavlína Miklánková[1], Eric Linster[1], Jean-Baptiste Boyer[2], Jonas Weidenhausen[3], Johannes Mueller[4], Laura Armbruster[1], Karine Lapouge[3], Carolina De La Torre[5], Willy Bienvenut[2], Carsten Sticht[5], Matthias Mann[4], Thierry Meinnel[2], Irmgard Sinning[3], Carmela Giglione[2], Rüdiger Hell[1], Markus Wirtz[1]*

In humans, the Huntingtin yeast partner K (HYPK) binds to the ribosome-associated N^{α}-acetyltransferase A (NatA) complex that acetylates ~40% of the proteome in humans and *Arabidopsis thaliana*. However, the relevance of *Hs*HYPK for determining the human N-acetylome is unclear. Here, we identify the *At*HYPK protein as the first in vivo regulator of NatA activity in plants. *At*HYPK physically interacts with the ribosome-anchoring subunit of NatA and promotes N^{α}-terminal acetylation of diverse NatA substrates. Loss-of-*At*HYPK mutants are remarkably resistant to drought stress and strongly resemble the phenotype of NatA-depleted plants. The ectopic expression of *Hs*HYPK rescues this phenotype. Combined transcriptomics, proteomics, and N-terminomics unravel that HYPK impairs plant metabolism and development, predominantly by regulating NatA activity. We demonstrate that HYPK is a critical regulator of global proteostasis by facilitating masking of the recently identified nonAc-X^2/N-degron. This N-degron targets many nonacetylated NatA substrates for degradation by the ubiquitin-proteasome system.

INTRODUCTION

N^{α}-terminal acetylation (NTA) is one of the most common protein modifications in eukaryotes. Up to 90% of soluble proteins are predicted to be N^{α}-terminally acetylated in humans and the reference plant *Arabidopsis* (*1*–*4*). In plants, NTA of specific substrates is executed post-translationally at the plasma membrane and after import of nuclear-encoded precursors into plastids (*5*–*7*). However, the bulk of proteins is N-terminally acetylated by four ribosome-associated N^{α}-acetyltransferase (Nat) complexes (NatA, NatB, NatC, and NatE) in a cotranslational manner in eukaryotes (*8*–*12*). Posttranslational and cotranslational NTA is required for the successful response of plants toward diverse environmental challenges (*7*, *9*, *10*, *12*, *13*). The key to the rapid acclimation of plants toward environmental cues is the remarkable plasticity of the plant proteome. One critical stress-responsive mechanism to dynamically adjust the steady-state level of a single protein is to regulate its destruction by the ubiquitin-proteasome system (*14*). Besides many other functions (*15*), NTA can control the stability of proteins by creating or masking N-terminally encoded degradation signals (N-degrons) that are recognized in humans and fungi by E3 ligases (N-recognins) (*16*, *17*). In plants, NTA stabilizes 8 of 10 tested cytosolic NatA substrates by masking the recently identified nonAc-X^2/N-degron (*18*).

The NatA complex is the dominant regulator of the N-acetylome in all eukaryotes, affecting approximately 40% of the proteome in humans and plants. NatA acetylates the N terminus of nascent polypeptide chains after the cleavage of the initiator methionine (iMet) by methionine aminopeptidase (MetAP), with a preference for the amino acids A, S, G, T, V, and C at the penultimate position (*10*, *19*). In all eukaryotes, the core NatA complex is composed of the ribosome-interacting subunit, NAA15 (N-alpha-acetyltransferase), and the catalytically active NAA10 subunit (*20*, *21*). In humans, *Drosophila melanogaster* (fruit fly), and *Saccharomyces cerevisiae* (yeast), this core NatA complex interacts with NAA50 (*22*, *23*). The plant *At*NAA50 regulates the endoplasmic reticulum stress response and is essential for plant fertility (*12*, *24*). However, whether *At*NAA50 interacts with the core NatA is still under debate (*24*, *25*).

The Huntingtin yeast partner K (HYPK) was first characterized as 1 of 15 proteins interacting with the human Huntingtin protein in a yeast two-hybrid screen (*26*). Crystal structures of the ternary NatA/HYPK of a thermophilic fungus (*Chaetomium thermophilum*) and the quaternary human NatA/NAA50/HYPK complex provide direct evidence for the interaction of HYPK and NatA complex in vitro (*27*, *28*). Biochemical characterization of *Hs*HYPK and *Ct*HYPK revealed that HYPK inhibits NatA in vitro (*28*, *29*). However, the depletion of HYPK in human cells did not increase the NTA frequency of NatA substrates. Instead, one canonical NatA substrate was even found to be substantially less acetylated, leaving the regulatory function of HYPK on NatA activity unresolved (*30*).

Here, we identify the plant HYPK ortholog and show that *At*HYPK facilitates NatA activity in planta. This discovery is corroborated by loss-of-HYPK lines that phenocopy the depletion of NatA core subunits with respect to global transcriptome alteration, stress resilience, and growth retardation. The absence of HYPK induces a substantial increase in global proteome turnover via activation of the ubiquitin-proteasome system. This massive protein breakdown is further evidenced by the destabilization of model reporter proteins containing the novel nonAc-X^2/N-degron that is masked in the wild type by NatA-mediated NTA. Our results identify HYPK as a critical regulator of NatA activity and global proteome stability in plants.

[1]Centre for Organismal Studies, Heidelberg University, Im Neuenheimer Feld 360, Heidelberg, Germany. [2]Université Paris-Saclay, CEA, CNRS, Institute for Integrative Biology of the Cell (I2BC), Gif-sur-Yvette, France. [3]Heidelberg University Biochemistry Center, Im Neuenheimer Feld, 328 Heidelberg, Germany. [4]Max-Planck-Institute for Biochemistry, Am Klopferspitz 18, Martinsried, Germany. [5]Center of Medical Research, Heidelberg University, Theodor-Kutzer-Ufer, Mannheim, Germany.
*Corresponding author. Email: markus.wirtz@cos.uni-heidelberg.de

RESULTS

Identification of HYPK in *Arabidopsis thaliana*

A search with the Basic Local Alignment Search Tool (BLAST) in the *Arabidopsis* proteome (Araport 11) using the human HYPK protein amino acid sequence (*Hs*HYPK, NP_057484) as query revealed the noncharacterized protein "Arabidopsis DNA-binding enhancer-like protein" (NP_566288.1) as the best candidate for the putative *At*HYPK protein (*E*-value: 1×10^{-15}). The protein encoded by At3g06610 displayed 62% amino acid coverage and 43% identity with *Hs*HYPK (fig. S1). The purified monomeric At3g06610-Strep II protein interacted with the Naa10/Naa15 complex from *C. thermophilum* in a ternary complex (Fig. 1A). Next, we tested the physical interaction of At3g06610 with NatA subunits in planta by applying the Split-luciferase system (*31*). Reconstitution of intact luciferase from two complementary nonactive fragments brought in close proximity due to fusion with At3g06610, *At*NAA15, and *At*NAA10 suggests that At3g06610 interacts with the core NatA subunits (Fig. 1B). Furthermore, we demonstrated the protein-protein interaction between *At*HYPK and *At*NAA15 with the yeast two-hybrid approach (fig. S2). On the basis of these data, we renamed "Arabidopsis DNA-binding enhancer-like protein" to "HYPK."

Loss of HYPK affects plant growth, stress resilience, and development

To address the biological function of HYPK in plants, we investigated three potential *HYPK* transferred DNA (T-DNA) insertion lines

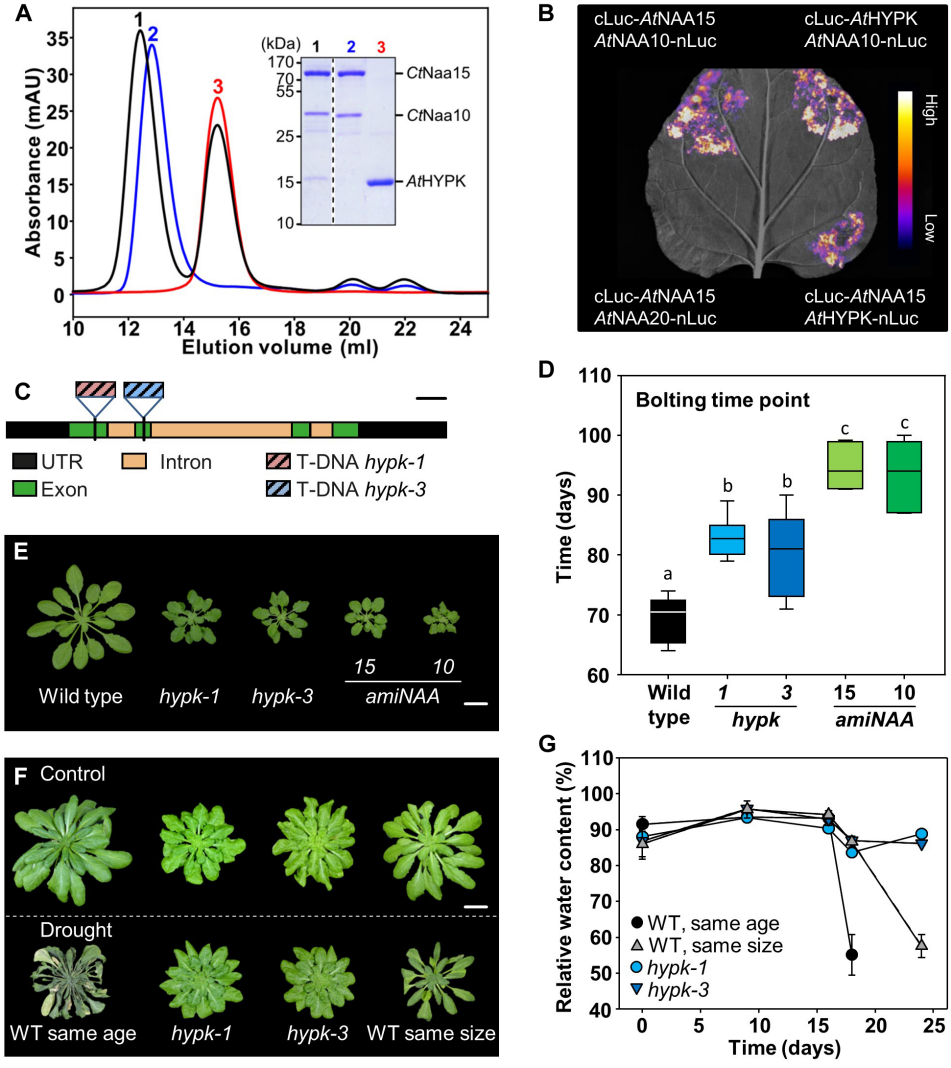

Fig. 1. Identification of *AtHYPK* and its impact on growth, development, and stress resilience. (**A**) Size exclusion chromatography of *At*HYPK-Strep II (3) and *Ct*NatA (2). The shift to lower elution volume demonstrates formation of *Ct*NatA-*At*HYPK-Strep II complex (1) and was verified by SDS–polyacrylamide gel electrophoresis (PAGE) (inset). (**B**) Reconstitution of luciferase after expression of cLuc-*At*HYPK and nLuc-*At*HYPK in combination with *At*NAA10-nLuc or cLuc-*At*NAA15. *At*NAA15-nLuc and cLuc-*At*NAA20 served as negative control. (**C**) Schematic representation of the T-DNA insertion in *hypk-1* and *hypk-3*. Scale bar, 100 bp. (**D**) Time point of bolting in *hypk*, *amiNAA10*, and *amiNAA15*. Data are given as median. The box represents the 15 to 85 percentile; the error bars indicate the percentiles 0 to 15 (lower) and 85 to 100 (upper). Different letters indicate individual groups identified by multiple pairwise comparisons with a Holm-Sidak, one-way analysis of variance (ANOVA) ($P < 0.01$, $n = 6$ to 8). (**E**) Phenotype of 6-week-old soil-grown wild-type, *hypk-1*, *hypk-3*, *amiNAA10*, and *amiNAA15* plants. Scale bar, 2 cm. (**F** and **G**) Representative phenotype (F) of control and drought-stressed *hypk-1*, *hypk-3*, and wild-type (WT) plants at the beginning (time point, 0) and after 24 days of the drought stress treatment. Scale bar, 2 cm. (G) The leaf relative water content of each genotype was determined at indicated time points. Data represent means ± SE ($n = 3$ to 4).

(fig. S3, A to E). The line *hypk-2* (SALK_083370.30.35) was wrongly annotated in The Arabidopsis Information Resource (TAIR, www.arabidopsis.org) as demonstrated by polymerase chain reaction (PCR)–based genotyping (fig. S3, C to E) and grew like the wild type. In contrast, a T-DNA insertion was located in the first exon of At3g06610 in *hypk-1* (SALK_083404_55.00) or the second exon in *hypk-3* (SALK_080671.32.70; Fig. 1C and fig. S3, F and G), prohibiting transcription of the full-length *HYPK* mRNA in both *hypk* lines. A fragmentary *HYPK* transcript containing the third exon was detectable in low amounts but not translated into functional HYPK protein in both lines, as demonstrated by liquid chromatography–tandem mass spectrometry (LC-MS^2)–based quantification (Table 1 and fig. S4). In contrast to *naa10-1* and *naa15-1* (*10*), *hypk-1* and *hypk-3* completed embryogenesis (Fig. 1, D and E). However, the absence of HYPK resulted in retarded vegetative growth of both lines (fig. S5A). Both *hypk* lines were indistinguishable from each other and resembled the phenotype of plants with decreased NatA activity (Fig. 1E). Like in NatA-depleted lines, the development of leaves and the switch from vegetative to generative growth were delayed in both hypk lines compared to wild type (Fig. 1D and fig. S5B). The hallmark of NatA-depleted plants is their resistance toward soil drying (*10*). Both hypk lines were also highly tolerant to soil drying compared to wild-type plants of the same developmental stage or the same age (Fig. 1F). Similar to NatA-depleted plants, *hypk* plants were drought resistant because of the increased formation of reactive oxygen species (ROS) in stomata resulting in constitutively closed stomata (fig. S5, C and D). Furthermore, *hypk* plants displayed an increased root/shoot ratio due to primary root growth promotion, allowing the plants to search in the soil's bottom layer for water (fig. S5, E and F). These constitutively induced drought-response pathways enabled *hypk* to maintain a regular relative water content for up to 24 days of water removal (Fig. 1G).

Table 1. Steady-state level of HYPK, NAA10, and NAA15 determined by nanoflow LC-MS^2–based quantification in soluble protein extracts of pooled roots from 7-week-old hydroponically grown wild-type, *hypk-1*, and *hypk-3* plants. Data represent means ± SE ($n = 4$) (HYPK peptide 1: [K].AFDKLTDRVEDR.[Q], HYPK peptide 2: [K].INPADVEFIVNELEIEK.[N], HYPK peptide 3: [R].VQSAMASIAASR.[E], HYPK peptide 4: [R].VQSAMASIAASR.[E]). The fourth peptide is oxidated on the methionine. a.u., arbitrary unit. Data for NAA10 and NAA15 represent the mean of 5 or 32 individual peptides, respectively. The number of biological replicates is given in brackets. Asterisks mark Kruskal-Wallis one-way ANOVA (*$P < 0.05$). These findings suggest that a twofold increase of NAA10 abundance does not complement the absence of HYPK in plants.

Signal intensity	Wild type	*hypk-1*	*hypk-3*
HYPK peptide 1 (a.u./10^4)	37 ± 6.9 ($n = 4$)	Not detectable	Not detectable
HYPK peptide 2 (a.u./10^4)	80 ± 31.7 ($n = 3$)	Not detectable	Not detectable
HYPK peptide 3 (a.u./10^4)	34 ± 4.6 ($n = 3$)	Not detectable	Not detectable
HYPK peptide 4 (a.u./10^4)	163 ± 15.7 ($n = 4$)	4 ($n = 1$ of 4)	Not detectable
NAA10 (*x*-fold of WT)	1 ± 0.13 ($n = 3$)	2.1* ± 0.22 ($n = 4$)	1.9* ± 0.14 ($n = 4$)
NAA15 (*x*-fold of WT)	1 ± 0.03 ($n = 4$)	1.1 ± 0.03 ($n = 4$)	0.6* ± 0.01 ($n = 4$)

HYPK promotes NatA activity in planta

Selective staining of free protein N termini revealed that both *hypk* lines accumulated soluble proteins displaying free N termini in comparable amounts as NatA-depleted plants (Fig. 2A). We applied the SILProNAQ global proteomics approach for proteome-wide assessment of the NTA frequency of individual proteins (*2*, *32*, *33*). Of the 419 unique N termini quantified in the *hypk* lines, 405 (97%) resulted from the cytosolic translation of nuclear genes, and 14 (3%) resulted from the translation of plastid-encoded genes. A total of 166 N termini (41%) were subject to iMet excision (NME), 51 (13%) proteins retained the iMet, and the remaining 188 protein N termini (46%) were caused by internal cleavage of proteins, predominantly occurring during maturation of nuclear-encoded mitochondrial or plastid proteins Proteomics Identifications Database (PRIDE, www.ebi.ac.uk/pride) (PRIDE ID: PXD023195).

An evident global decline of N-terminal acetylation was observed in both *hypk* lines. The average acetylation yield of the whole dataset was decreased by 12 ± 1% (PXD023195). This increase of nonacetylated proteins in *hypk* lines was triggered by the significantly decreased NTA of NatA substrates (27 ± 3%), characterized by iMet excision before acetylation of the penultimate amino acid (Fig. 2B). Loss of HYPK affected NatA substrates displaying either A, G, S, or T at the neogenerated N terminus. The extent of the impact of both *hypk* lines on single entries of the fully acetylated subset of the wild type is displayed in fig. S6A. The data indicate that the HYPK knockout is similar in each line within the error bar and that the decrease is similar in most entries.

In contrast, the absence of HYPK did not impair the distribution of NTA yield of proteins retaining the iMet at their N terminus (Fig. 2C), which includes canonical NatB substrates (fig. S6B) and the NatC/NatE/NatF substrates (fig. S6C). The *hypk* lines displayed wild type–like NTA yield on proteins subject to internal cleavage (e.g., post-translationally matured organelle-localized proteins; Fig. 2D) or were translated in the plastids (fig. S6D). Loss of HYPK resulted in a decrease of acetylation of the NatA substrates comparable to the down-regulation of NatA activity by depleting the core NatA complex subunits in *amiNAA15* or *amiNAA10* mutants (Fig. 2, E and F). This finding is consistent with the highly similar phenotype of *hypk* lines and NatA-depleted plants (Fig. 1, D to G).

Next, we determined transcript and protein abundance of the core NatA complex subunits to rule out that loss of HYPK caused codown-regulation of its protein-interaction partners. Neither transcript nor protein levels of NAA10 and NAA15 were significantly decreased in both *hypk* lines when compared to wild type (Table 1 and fig. S4). The catalytically active NAA10 protein even accumulated approximately twofold in roots of both *hypk* lines, potentially because of a feedback mechanism trying to compensate for decreased in vivo NatA activity in these lines (Table 1 and Fig. 2B; PRIDE ID: PXD023599). These findings demonstrate that loss of HYPK explicitly decreases the activity of the cotranslationally acting NatA complex but does not decrease the abundance of the core NatA subunits. Noticeably, HYPK depletion did not impair the NTA frequency of proteins addressed by the other ribosome-associated Nats.

The HYPK function is conserved in higher eukaryotes

To provide direct evidence for the regulatory function of HYPK in plants and to test for the evolutionary conservation of HYPK function

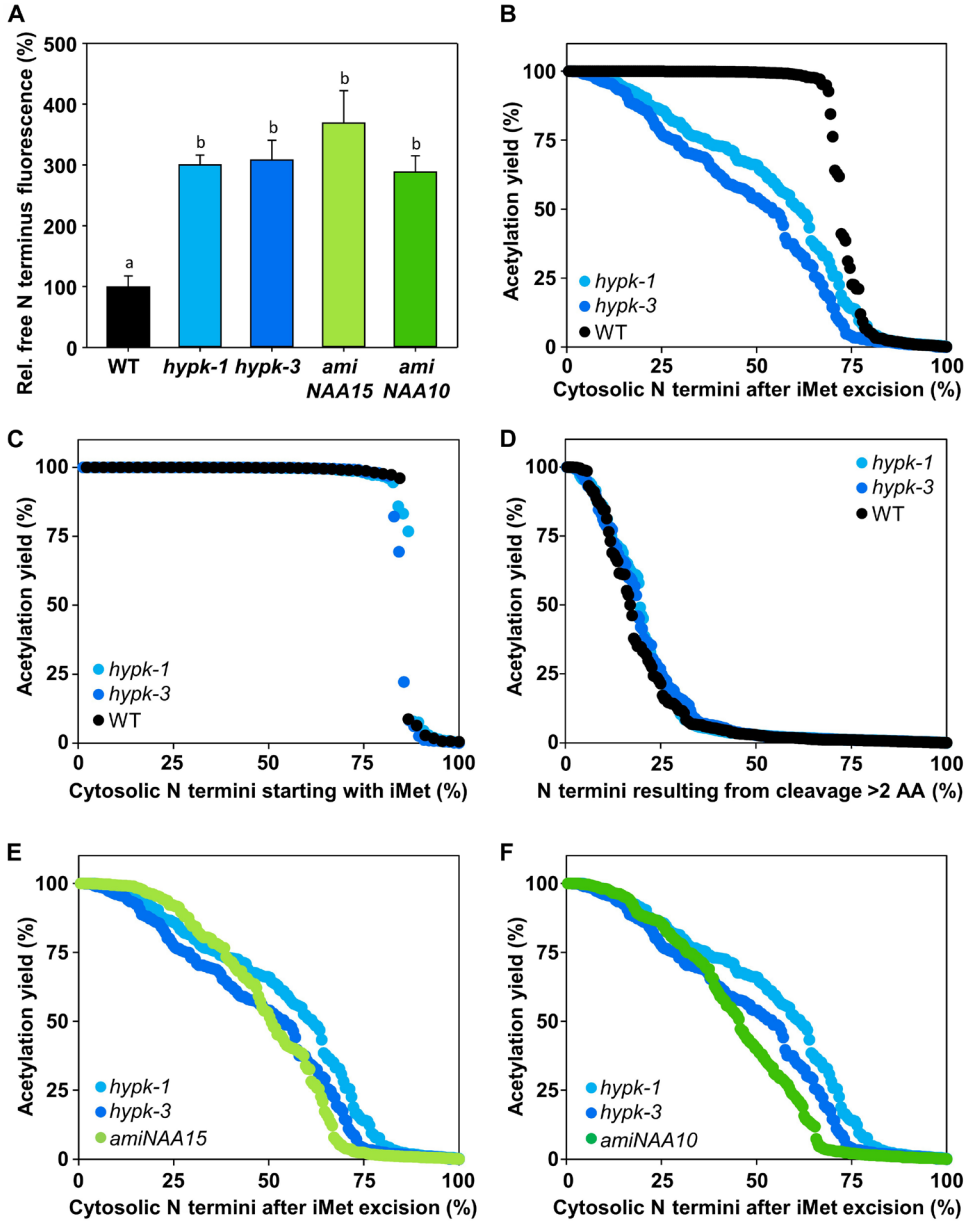

Fig. 2. HYPK regulates NTA of the NatA substrates. (**A**) Quantification of the relative global amount of free N termini in soluble protein extracts isolated from leaves of 6-week-old plants as determined by staining with the fluorescent dye NBD-Cl. Data are given as means ± SE. Different letters indicate individual groups identified by multiple pairwise comparisons with a Holm-Sidak one-way ANOVA ($P < 0.05$, $n = 4$). (**B**) Level of N-terminally acetylated protein peptides after excision of the iMet in 6-week-old wild-type (WT) and *hypk-1* and *hypk-3* mutants that are lacking HYPK (*hypk-1*: $N = 191$, *hypk-3*: $N = 193$, and WT: $N = 177$). (**C**) Acetylation level of protein peptides starting with the iMet (*hypk-1*: $N = 75$, *hypk-3*: $N = 76$, and WT: $N = 45$). (**D**) Acetylation level of protein peptides that are produced by internal cleavage, e.g., matured mitochondrial and plastid proteins (*hypk-1*: $N = 265$, *hypk-3*: $N = 253$, and WT: $N = 212$). (**E** and **F**) Levels of N-terminally acetylated protein peptides after excision of the iMet in *hypk* and *amiNAA15* or *amiNAA10* (*hypk-1*: $N = 191$, *hypk-3*: $N = 193$, *amiNAA15*: $N = 201$, and *amiNAA10*: 280).

in eukaryotes, we independently complemented three *hypk-3* plants with Strep-tagged *At*HYPK (Strep-*At*HYPK) under control of the 35*S* promoter. Strep-*At*HYPK–complemented *hypk-3* lines grew similar to the wild type (Fig. 3, A and B, and fig. S8) and displayed wild type–like levels of free protein N termini (Fig. 3C). The expression of Strep-tagged human HYPK (Strep-*Hs*HYPK) from the same construct also entirely rescued the decreased growth phenotype and reversed the number of proteins displaying free N termini in *hypk-3* to a wild type–like level (Fig. 3, D to F, and fig. S8, D and E). *hypk-3* mutants expressing Strep-tagged HYPK from the fungus *C. thermophilum* (Strep-*Ct*HYPK) grew better than *hypk-3* but not like the wild type (Fig. 3, D and E, and fig. S8, D and E), which is consistent with the only partial recovery of the proteins displaying free N termini in Strep-*Ct*HYPK–complemented *hypk-3* (Fig. 3F). This partial complementation of *hypk-3* plants grown at ambient temperature might be explained by a lowered biological activity of the *Ct*HYPK protein,

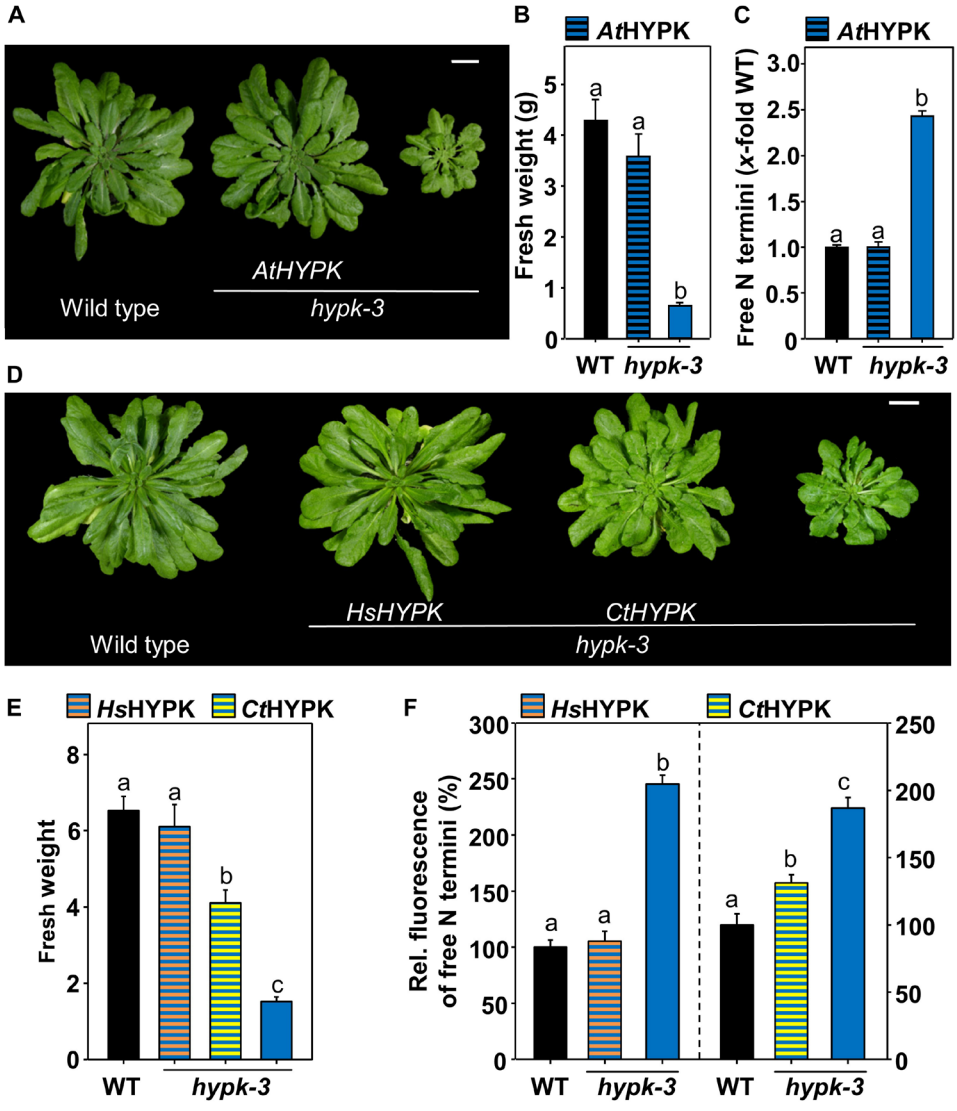

Fig. 3. Loss of *At*HYPK in plants can be complemented by expression of HYPK from *Arabidopsis*, humans, or *C. thermophilum*. (**A** to **C**) Habitus (A), fresh weight (B), and level of free N termini (C) of 9.5-week-old soil-grown wild-type (WT; black), *hypk-3* (dark blue), and *hypk-3*–expressing Strep-*At*HYPK (dashed black). (**D** to **F**) Habitus (D), fresh weight (E), and level of free N termini (F) of 10-week-old soil-grown wild type (WT; black), *hypk-3* (dark blue), and *hypk-3*–expressing Strep-*Hs*HYPK (dashed red) or Strep-*Ct*HYPK (dashed yellow). Data are represented as means ± SE. Different letters indicate individual groups identified by multiple pairwise comparisons with a Holm-Sidak, one-way ANOVA ($P < 0.05$, $n = 4$ to 10). Scale bar, 2 cm.

which is optimized during the evolution of *C. thermophilum* to function at 50° to 55°C or by different codon usage of thermophilic fungi in comparison to plants.

Loss of HYPK induces the ubiquitin-proteasome system

To test whether HYPK affects plant metabolism and development exclusively by lowering NatA activity, we compared the transcriptome changes of *hypk-3* and *hypk-1* with the transcriptome changes induced by depletion of the catalytically active subunit of the NatA complex (Gene Expression Omnibus accession: GSE158586). The depletion of NAA10 caused the most substantial perturbation in gene expression compared to wild type, with 1503 and 1641 genes significantly up- and down-regulated. Approximately 1000 genes were either significantly up- or down-regulated in both *hypk* lines (Fig. 4, A and B, and table S1). The vast majority of these regulated genes (~75%) were coregulated in *hypk* lines and *amiNAA10* (Fig. 4, A and B, intersection). We did not find any gene that was antagonistically regulated in both *hypk* lines when compared to *amiNAA10* (Fig. 4, C and D). A comparative gene set enrichment analysis (GSEA) revealed that the same pathways were affected by the loss of HYPK or NAA10 depletion (table S2). These results strongly suggest that the loss of HYPK predominantly affects plant metabolism by decreasing NatA activity.

The GSEA of regulated genes in *hypk* lines revealed that loss of HYPK induced transcription of genes involved in autophagy, proteasome, ubiquitin-mediated proteolysis, and protein processing in the endoplasmic reticulum (table S2). To provide further evidence for the ubiquitin-proteasome system induction, we quantified the steady-state levels of polyubiquitinated proteins in the wild type and both *hypk* lines in the presence or the absence of the proteasome inhibitor

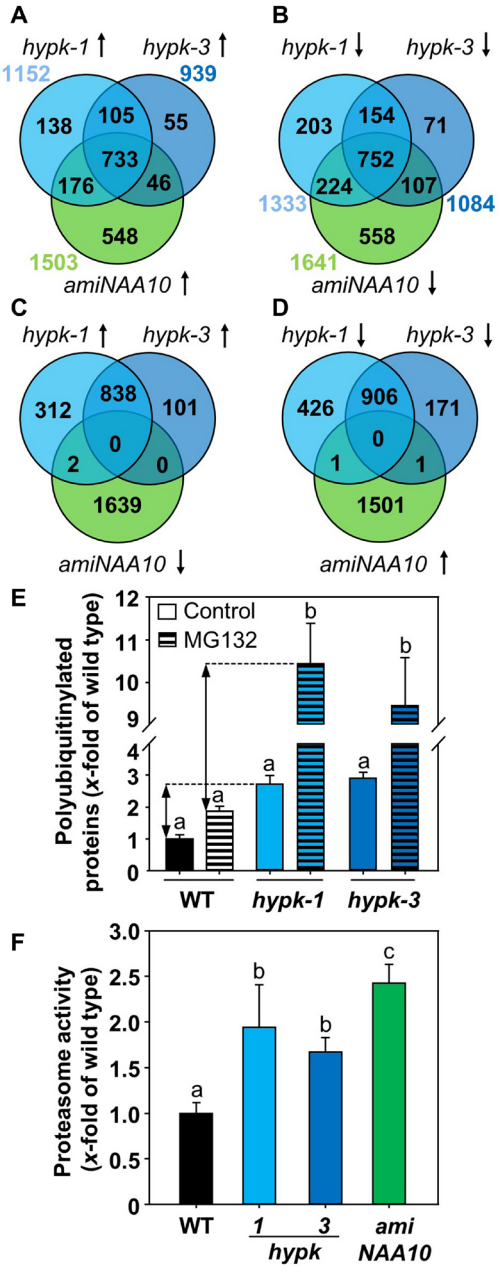

Fig. 4. Depletion of HYPK or NatA activity induces similar transcriptional responses and activates the ubiquitin-proteasome system. (**A** to **D**) Venn diagrams of significantly regulated transcript steady-state levels ($P < 0.05$, >1.5-fold) in mutants that are lacking HYPK or are depleted of NAA10 (*amiNaa10*) when compared to wild type. Most of the transcripts are coregulated in *hypk-1*, *hypk-3*, and *amiNAA10* [(A) up-regulated transcripts: ↑; (B) down-regulated genes: ↓]. The total number of significantly regulated genes is shown outside the Venn diagram. No transcript that was significantly up-regulated (B) or down-regulated (D) in both *hypk* lines was antagonistically regulated in *amiNAA10*. (**E**) Relative levels of polyubiquitinated proteins in leaves of 6-week-old soil-grown wild-type (WT; black), *hypk-1*, and *hypk-3* plants (blue) treated without (control) or with 50 μM MG132 (MG132, dashed) to inhibit the proteasome. Arrows indicate fold induction of polyubiquitinated proteins between wild type and *hypk-1* in the absence or presence of MG132. (**F**) Relative proteasome activity in leaves of 6-week-old wild type (WT), *hypk-1*, *hypk-3*, and *amiNaa10*. Data are represented as means ± SE. Different letters indicate individual groups identified by pairwise multiple comparisons with a Holm-Sidak, one-way ANOVA [$P < 0.05$, $n = 3$ to 4 (E); $P < 0.05$, $n = 4$ (F)].

MG132. When the proteasome was functional, the level of polyubiquitinated proteins was threefold higher in *hypk* plants than in wild-type plants. However, when we inhibited the proteasome, this increase was more pronounced (Fig. 4E and fig. S9), suggesting that an elevated in vivo proteasome activity quickly degraded polyubiquitinated proteins in *hypk* lines. The extractable proteasome activity was significantly enhanced in *hypk* lines compared to wild type and increased to similar levels as in NatA-depleted plants (Fig. 4F) (*18*).

HYPK is critical for the stabilization of NatA substrates

Induction of in vivo ubiquitination rates and the proteasome suggested significantly higher protein destruction capacity in *hypk* lines. For that reason, we quantified the global protein degradation rates in leaves of *hypk* lines, *amiNAA10,* and the wild type after feeding of ^{35}S-labeled cysteine and methionine. The loss of HYPK or depletion of NatA activity substantially enhanced the protein degradation rate as determined by the decrease of the isotope label in the protein fraction after inhibition of translation with cycloheximide (Fig. 5A). Despite the up to 5.7-fold faster protein degradation, the total level of extractable soluble proteins and the abundance of distinct proteins were unaffected in *hypk* lines (fig. S10). A shotgun proteomics approach confirmed that of the 1253 proteins detected in the wild-type and *hypk* lines (table S3; PRIDE ID: PXD022120), only 31 proteins were significantly [permutation-based false discovery rate (FDR) ≤ 0.05] decreased (<0.67-fold) in *hypk-1 or hypk-3* (Fig. 5, C and D). Of these lower abundant proteins, 81 and 94% were canonical NatA substrates (table S4; Fisher's exact test, $P < 0.0001$ for the enrichment of NatA substrates in the subset of lower abundant proteins in *hypk* lines), strongly suggesting that lowered NTA of these NatA substrates caused their destabilization. In a companion study (*18*), we demonstrated that decreased NatA activity resulted in a faster turnover of NatA substrates and identified the novel nonAc-X^2/N-degron targeting nonacetylated NatA substrates for degradation. On the basis of the findings in *hypk-3* and the knowledge of the NTA-mediated stabilization of NatA substrates, we suggested that the destabilization of many other NatA substrates is compensated by enhanced translation of these proteins to maintain their steady-state level in *hypk* plants. Incorporation of isotope-labeled amino acids into proteins revealed a substantially enhanced global translation in *hypk* plants (Fig. 5B), demonstrating a considerable increase in global protein turnover when HYPK is absent in plants. To provide evidence for enhanced turnover of nonacetylated NatA substrates in *hypk* lines, we quantified the protein half-life time of eight model nonAc-X^2/N-degron–containing proteins in *hypk* plants by application of the tandem Fluorescent Protein Timer (tFT) approach (*34*). All tested model nonAc-X^2/N-degron–containing proteins [e.g., ^{SIS}CCT1 (AT3G20050)] were destabilized in *hypk* plants (Fig. 6, A and B, and fig. S11 to S17). Next, we genetically engineered a nonacetylated version of the ^{SIS}CCT1 protein by integrating a proline after the acetylated S^2 (^{SPI}CCT1). The nonacetylated ^{SPI}CCT1 was destabilized in the wild type when compared to the native ^{SIS}CCT1. ^{SPI}CCT1 displayed the same stability in the wild type and the *hypk-3* mutant (Fig. 6, A and B). The latter finding unambiguously demonstrated that the destabilizing effect of HYPK on the native ^{SIS}CCT1 is caused by lowering its NTA frequency and not by a pleiotropic effect. The non-NatA substrates ^{MPP}SAT5 (AT1G55920) and ^{MRE}TUBB4 (AT5G44340) (Fig. 6, A and B) were stable in *hypk* mutants, suggesting that the enhanced global protein turnover in *hypk* was predominantly triggered by destabilization of nonacetylated

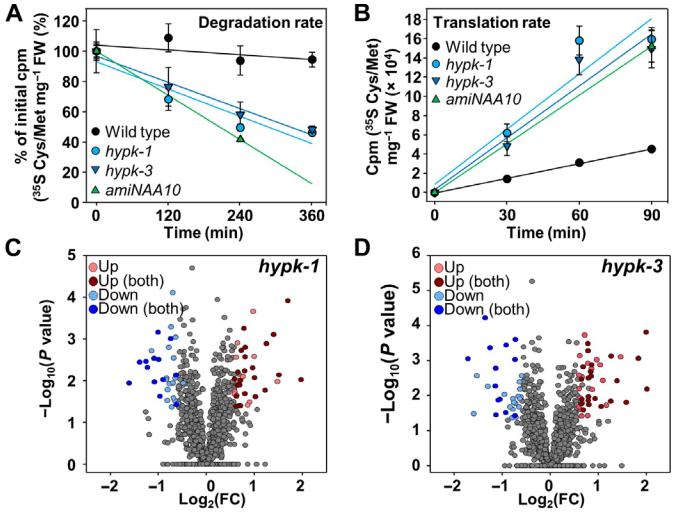

Fig. 5. HYPK affects global protein turnover. (**A**) Degradation rate of soluble proteins from leaf discs of 7-week-old wild-type, *hypk* and *amiNAA10* plants. Isotope-labeled sulfur amino acids were incorporated into the proteins for 17 hours; subsequently, the translation was stopped for 6 hours by the addition of 1 mM cycloheximide (time point, 0). Free amino acids were removed, and the remaining radioactively labeled proteins were detected with a scintillation counter at indicated time points. FW, fresh weight. (**B**) Translation rate of soluble proteins in leaves of 7-week-old wild-type, *hypk*, and *amiNaa10* lines. Isotope-labeled sulfur amino acids were incorporated into newly synthesized proteins for 90 min, and samples were collected at indicated time points. The level of isotope-labeled proteins was quantified after the removal of free amino acids by size exclusion chromatography. Data represent means ± SE ($n = 4$). cpm, counts per minute. (**C** and **D**) Steady-state levels of soluble proteins in *hypk-1* (C) or *hypk-3* (D) when compared to wild type. Gray spheres in the volcano plots represent unchanged proteins, while significantly altered proteins are indicated by color (decreased in both *hypk* lines, dark blue; decreased in only one genotype, light blue; increased in both *hypk* lines, dark red; decreased in only one genotype, light red; >1.5-fold when compared to wild type, $P < 0.05$). Data are represented as means ($n = 4$). FC, fold change.

NatA substrates containing a nonAc-X^2/N-degron. In support of this view, NatA substrates lacking a nonAc-X^2/N-degron, such as CYP19 (Cyclophilin 19) and UGE1 (UDP-D-Glucose/UDP-D-Galactose 4-Epimerase 1), were not affected in *hypk-3* (Fig. 5F and figs. 18 and 19).

DISCUSSION

The NatA complex acetylates 40% of the proteome in higher eukaryotes in a cotranslational manner when 40 amino acids have emerged from the exit tunnel (*20*). The catalytically active NAA10 requires ribosome anchoring by its accessory subunit NAA15 for in vivo activity on proteins displaying Ala, Ser, Gly, Thr, and Val of nascent chains (*1*, *10*, *21*). Consequently, the cotranslational removal of the iMet by MetAP is a prerequisite for the recognition of substrates by NatA at the ribosome (*35*). The area above the ribosome exit tunnel is a highly crowded environment because diverse ribosome-associated factors compete to act on the extruding nascent chain (*36*). How the NatA complex and the MetAP action are concerted in a spatiotemporal manner to allow for efficient NTA of the diverse NatA targets is currently unknown. Here, we identify the NAA15-interacting protein HYPK (Fig. 1) as a critical promotor of NatA activity in plants. The absence of HYPK did not affect iMet removal by MetAP but exclusively inhibited NTA of substrates displaying various N termini starting with Ala, Ser, Gly, and Thr in vivo (Fig. 2B and fig. S6A). Interaction of HYPK with the NatA complex does not require the ribosome (Fig. 1A) (*28*), implying that the ternary NatA/HYPK complex can associate before the ternary complex transiently interacts with the ribosome for recognition and acetylation of NatA substrates. HYPK has an intrinsic chaperone-like function, which allows it to prevent other proteins' aggregation by binding to aggregation-prone disordered regions of proteins (*37*, *38*). These features of HYPK would be well suited to allow spatial orientation of the nascent chain in the crowded area above the ribosome exit tunnel and potentially selective transfer of the neo-generated N termini from MetAP to NatA. In this context, it is remarkable that the overall probability of being N-terminally acetylated by NatA is significantly higher for proteins with N-terminally disordered regions (*39*). A global function of HYPK as a general scaffold stabilizing nascent chains extruding from the ribosome exit tunnel is unlikely in plants because the activities of other ribosome-associated *N*-acetyltransferases were not impaired by loss of HYPK (Fig. 2, C and D, and fig. S6, B and C).

In the absence of the ribosome, HYPK of *C. thermophilum* and humans substantially inhibit NAA10 in the ternary NatA/HYPK complex due to distortion of the NAA10 active site or blocking the active sites by their conserved N-terminal loop-helix regions (*28*, *29*). This intrinsic inhibitory function of HYPK might help in vivo to restrict the action of NatA to nascent chains extruding from the ribosome because it prevents NTA of neo-generated NatA substrates that arise from proteolytic cleavage processes in the cytosol. Some of these proteolytic cleavage products are short-lived signal peptides in plants (*40*) and thus should not be stabilized by NTA (see below the formation of nonAc-X^2/N-degrons).

The binding of plant HYPK to the *Ct*NatA complex in vitro (Fig. 1A) and the capability of *Ct*HYPK and *Hs*HYPK to complement the loss of plant HYPK in vivo (Fig. 3) demonstrate significant evolutionary conservation of HYPK function in eukaryotes. This view of an evolutionarily conserved action of HYPK in the ternary NatA/HYPK complex is reinforced by the lowered NTA of the NatA substrate PCNP (PEST proteolytic signal-containing nuclear protein) in human cells depleted of HYPK and the combined action of HYPK and NatA to prevent aggregation of a Huntingtin protein variant (*30*). In humans, self-oligomerized amorphous HPYK is supposed to sense protein aggregation and prevent toxic protein aggregates by forming a sequestration complex (*41*). Comparative analyses of the phenotype, the stress resilience, the transcriptome, the proteome, and the N-terminome of *hypk* and NatA-depleted plants revealed no substantial indication for a function of HYPK outside of the ternary NatA/HYPK complex in plants. However, in contrast to the core subunits of NatA (*10*), HYPK is not essential for the embryogenesis of *Arabidopsis*. The viability of *hypk* mutants suggests that, unlike the ribosome-anchoring subunit NAA15 (*10*, *11*, *42*), HYPK is not essential for in vivo activity of NAA10 on all NatA substrates. This finding is consistent with identifying many partially NTAed NatA substrates in *hypk* mutants (Fig. 2B and fig. S6A).

Loss of HYPK causes a significant induction of the ubiquitin-proteasome system and significantly enhances the global protein turnover in plants (Figs. 4E and 5, A and B). In NatA-depleted plants, such an increased global protein turnover was also observed and caused by constitutively higher Target of Rapamycin (TOR) activity (*18*). Consequently, the increased protein turnover in *hypk* lines can be attributed to the NatA activity–promoting function of HYPK

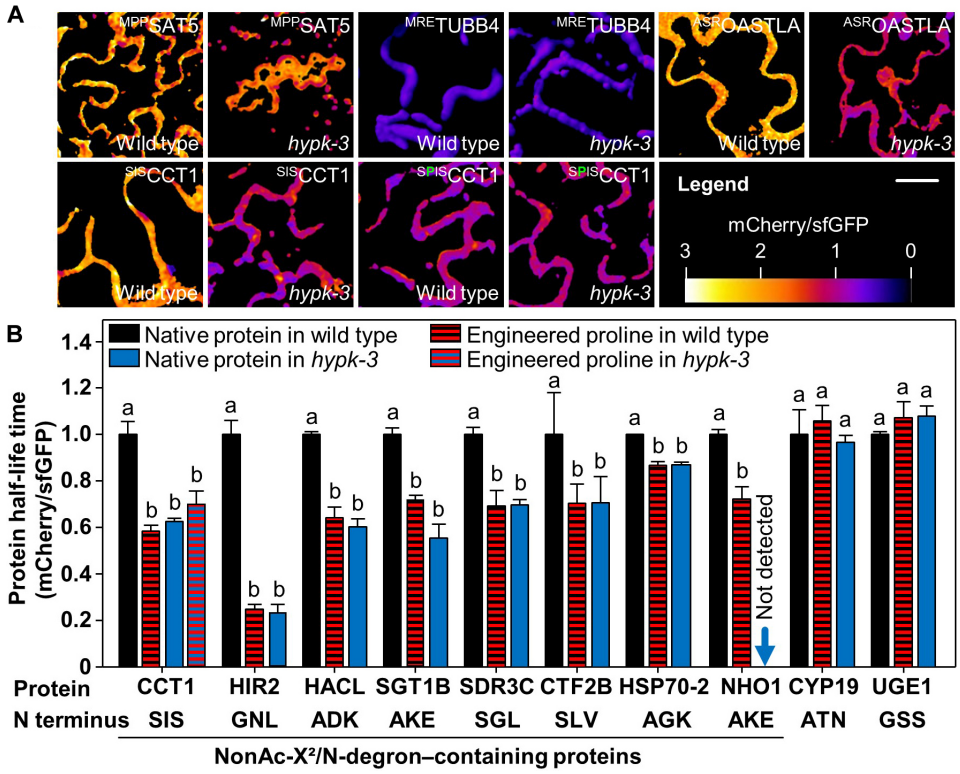

Fig. 6. HYPK affects stability of nonAc-X^2/N-degron containing NatA substrates. (**A**) Noninvasive in vivo determination of relative protein half-life times in the wild-type and *hypk-3* plants after fusion of selected proteins with the tFT consisting of the slow maturing mCherry and the quickly maturing superfolding green fluorescent protein (sfGFP). False-color images represent the ratio of mCherry to sfGFP fluorescence in pavement cells after transient transformation of *Arabidopsis* leaves. The mCherry/sfGFP signal intensity ratio correlates positively with the relative half-life time of the POI-tFT polypeptide chain. Proteins that are not targeted by the NatA complex (^{MPP}SAT5 and ^{MRE}TUBB4) display indistinguishable stability in the wild type and *hypk-3*. The canonical NatA substrates (^{ASR}OASTLA and ^{SIS}CCT1) are significantly destabilized in *hypk-3*. CCT1 is also destabilized by inhibition of NTA in the wild type due to the introduction of a proline at position 3 (^{SPIS}CCT1). The ^{SPIS}CCT1-tFT protein is not further destabilized in *hypk-3*, demonstrating that CCT1 is destabilized in plants because of absent NTA. (**B**) Quantification of 10 selected NatA substrates (including CCT1) demonstrate that all previously identified nonAc-X^2/N-degron containing proteins (*18*) are destabilized in *hypk-3*. Data represent the means ± SE. Different letters indicate individual groups identified by pairwise multiple comparisons with a Holm-Sidak, one-way ANOVA ($P < 0.05$, $n = 3$ to 8).

at the ribosome. We provide direct evidence that HYPK controls the stability of nonAc-X^2/N-degron–containing proteins by promoting NTA of NatA substrates. It remains to be elucidated if the enhanced protein turnover in *hypk* is also caused by aggregation of nonacetylated proteins as suggested in yeast *natA* mutants (*39*) or generation of orphaned proteins (*16*). However, noninvasive protein turnover analysis of NatA substrates revealed no indication for significant formation of protein aggregates or protein misallocation when the nonAc-X^2/N-degron–containing NatA substrates were not cotranslationally imprinted with an acetylation mark (Fig. 5 and figs. S11 to S18) (*18*). Because abscisic acid (ABA) dynamically down-regulates NatA transcription and NatA protein abundance, stimulus-induced increase of proteins harboring a free N terminus might help to replace stress-damaged proteins and add to protein surveillance as suggested earlier (*16*).

Albeit the function of NAA10 and HYPK for imprinting of the proteome with acetylation marks is conserved between *Arabidopsis* and humans, it is currently less clear whether NTA of nonAc-X^2/N-degron containing NatA substrates also serves as a stabilizing signal in animals (*43*, *44*). However, several N-recognins that specifically recognize nonacetylated NatA substrates or proteins displaying a nonmodified G^2/N-degron have been recently identified in humans (*45*, *46*). Furthermore, the ^{GAV}THOC7 protein is stabilized by the N-terminal acetylation of the GLY^2 (*47*). In agreement with these recent findings, our data demonstrate that plant HYPK is a critical promotor of ribosome-associated NatA activity and can determine the half-life time of NatA substrates by facilitating the cotranslational masking of the pervasive nonAc-X^2/N-degron, when these proteins are extruded from the ribosome exit tunnel.

MATERIALS AND METHODS

Search for HYPK in *Arabidopsis* proteome

The *Homo sapiens* HYPK protein [NP_057484; (*30*)] was used as a query in the blastp program (National Center for Biotechnology Information; https://blast.ncbi.nlm.nih.gov/Blast.cgi?PAGE=Proteins) to search for the HYPK protein in *A. thaliana*. Input settings of blastp were as follows: expect threshold, 10; word size, 6; alignment matrix score, BLOSUM62; gap costs, existence, 11; extension: 1.

Plant material and growth

All analyzed plants belong to the *A. thaliana* ecotype Col-0. The here analyzed T-DNA insertion lines *hypk-1* (SALK_083404_55.00) and *hypk-3* (SALK_080671.32.70) were obtained from NASC (www.arabidopsis.info). Plants were germinated and grown on soil [Tonsubstrat (Ökohum, Herbertingen)] supplemented with 10% (v/v)

vermiculite and 2% (v/v) quartz sand. Seeds were stratified for 2 days on humid soil at 4°C in the dark and then transferred to short-day conditions (8.5-hour day, light intensity: 70 to 100 µmol m^{-2} s^{-1}; day temperature: 22°C; night temperature: 18°C; relative humidity: 50 to 60%) in plant growth chambers (Waiss). Plants were kept under short-day conditions for time-resolved quantification of growth by measuring rosette size and determination of the bolting time. The radius of the rosette was determined in triplicate, and values were averaged. For seed production, 8-week-old soil-grown plants were transferred to long-day conditions (16-hour light per day; other conditions were the same as in short-day cultivation) and grown until seeds matured in the siliques.

Seeds for hydroponic cultivation were sterilized in 70% ethanol (2 min) followed by a treatment for 10 min in 6% hypochlorite. Seeds were then washed five times with sterile double-distilled H_2O (ddH_2O) and stratified for 2 days at 4°C in the dark on solid ½ Hoagland solution [2.5 mM $Ca(NO_3)_2$, 0.5 mM $MgSO_4$, 2.5 mM KNO_3, 0.5 mM KH_2PO_4, 4 µM Fe-EDTA, 25 µM H_3BO_3, 2.25 µM $MnCl_2$, 1.9 µM $ZnCl_2$, 0.15 µM $CuCl_2$, 50 nM $(NH_4)_6Mo_7O_{24}$, and 0.6% (w/v) microagar (pH 5.8)]. The seedlings were grown in growth cabinets (Percival Intellus, Laborgeräte GmbH) under short-day conditions (8-hour light, 120 µmol m^{-2} s^{-1}; day/night temperature: 22°/18°C) for 2 weeks. Seedlings were then transferred to hydroponic conditions and further grown in a liquid ½ Hoagland solution (*48*).

Quantification of the drought stress response

Individual plants were cultivated under short-day conditions for 5 weeks in a pod containing identical soil amounts. At this time point, the watering was stopped for the drought-stressed plants and continued for control plants. Relative water content in the leaves was determined at different time points as described in (*10*).

Determination of stomatal aperture

The stomatal aperture was measured on the abaxial side of 6-week-old soil-grown plants under confocal laser-scanning microscope A1R (Nikon). Quantification of the aperture was performed with Fiji software.

Determination of ROS production in stomatal guard cells

ROS production was quantified in the stomatal guard cells on the epidermal peels of 6-week-old plants according to (*10*) with slight modifications. To obtain ABA-induced ROS production, peels were incubated with ABA for 1 hour before H_2O_2 staining. H_2O_2 staining was performed for 20 min, and peels were washed in ddH_2O for 15 min.

Determination of root/shoot ratio

Plants were grown hydroponically for 6 weeks, rosette radius was measured in three dimensions, and the length of the complete root was determined. Roots were dried from the excessive liquid and weighed.

Extraction of genomic DNA, PCR, genotyping, and cloning

For PCR-based genotyping of plants, genomic DNA (gDNA) was extracted from leaves according to (*49*). The gDNA served as a template for the amplification of distinct alleles with specific primers defined in table S5 using the FastGene TAQ Ready Mix PCR Kit (Nippon Genetics).

For the creation of HYPK overexpression constructs, the HYPK open reading frames (orfs) were PCR-amplified from complementary DNA (cDNA) libraries of the respective organism using the PCRBIO HiFi Polymerase (PCRBIOSYSTEMS) and specific primers encoding the Strep-tag (table S5). The resulting PCR fragments (Strep-*At*HYPK, Strep-*Hs*HYPK, and Strep-*Ct*HYPK) were subcloned into pDONR201 vector (Gateway system) and transferred by Gateway cloning into pB7YWG2 vector. All final vectors were sequenced to confirm sequence identity (EUROFINs).

Determination of protein-protein interaction

To test the physical interaction of *At*HYPK with the NatA complex, the previously purified *Ct*NatA complex (*28*) was used. After PCR-supported cloning of *At*HYPK with specific primers (table S5) into the pET24d vector (Novagen), the His_6–glutathione *S*-transferase (GST)–tobacco-etch-virus (TEV)–*At*HYPK-Strep II protein was expressed in Rosetta II (*DE3*) *Escherichia coli* cells. After extraction, His_6-GST-TEV-*At*HYPK-Strep II was purified by immobilized metal affinity chromatography (IMAC) on His-trap FF column (GE Healthcare) according to the manufacturer's instructions [20 mM Hepes (pH 8.0), 250 mM NaCl, and 20/250 mM imidazole]. TEV protease cleavage of the His6-GST carrier was performed during dialysis overnight at 4°C in dialysis buffer [20 mM Hepes (pH 8.0), 250 mM NaCl, and 15 mM imidazole] and reverse IMAC removed His6-GST and TEV protease. *At*HypK-Strep II was further purified by size exclusion chromatography using a Superdex 200 26/60 gel filtration column (GE Healthcare) in buffer G [20 mM Hepes (pH 8.0) and 250 mM NaCl]. A total of 8 µM *Ct*NatA was incubated with 90 µM *At*HypK-Strep II at 4°C for 1 hour in 20 mM Hepes (pH 8.0) and 250 mM NaCl. Proteins were injected onto a Superdex 200 10/300 GL gel filtration column (GE Healthcare). The differences in the elution profiles of *Ct*NatA, *At*HypK-Strep II, and the *Ct*NatA-*At*HypK mix were analyzed, and SDS–polyacrylamide gel electrophoresis (SDS-PAGE)–separated proteins in the peak fractions were visualized by Coomassie staining.

To test the physical interaction of *At*HYPK with the NatA ribosome anchoring subunit *At*NAA15, the yeast two-hybrid approach was applied as described in (*25*). *At*NAA15 and *At*HYPK were cloned into the vectors pG4BDN22::*At*NAA15 and pG4ADC111::*At*HYPK after PCR amplification with specific primers (table S5). Both vectors were cotransformed in the yeast strain PJ69-4A, and transactivation controls were systematically performed for each construct.

Firefly luciferase complementation imaging assay

For in planta detection of protein-protein interactions, the full-length cDNA sequences of *At*NAA10 (AT5G13780), *At*NAA15 (AT1G80410), *At*NAA20 (AT1G03150), and *At*HYPK (AT3G06610) were amplified with specific primers (table S5) and fused upstream of N-Luc in the pCambia-NLuc and downstream of C-Luc in the pCambia-CLuc vector system (*31*). The resulting vectors were transformed into the *Agrobacterium tumefaciens* strain GV3101. Subsequently, the cotransformation of both vectors into *Nicotiana benthamiana* leaves was performed as described in (*50*). After 3 days, the abaxial sides of leaves were anointed with luciferin (1 mM) and incubated in the dark for 5 min. The luciferase signal was detected with the ImageQuant LAS 4000 at the binning set to 8 × 16 pixels for up 15 min.

Determination of steady-state transcript levels

Total leaf RNA was extracted with the peqGOLD Total RNA Kit (peqlab) followed by DNA digestion with the DNase I Digest Kit (VWR). Transcript steady-state levels of selected genes were analyzed

by reverse transcription quantitative (RT-qPCR) as described in (*9*) with specific primers listed in table S5.

Whole-transcriptome analysis

For gene expression profiling, total RNA was extracted as described above and converted to biotinylated antisense cDNA according to the Affymetrix standard labeling protocol. The resulting cDNA was hybridized to the Arabidopsis AraGene-1_0-st-type (Affymetrix) as described in (*10*).

A Custom CDF Version 20 with TAIR-based gene definitions was applied for array annotation (*51*). Raw intensity values were RMA background corrected and quantile normalized. One-way analysis of variance (ANOVA) was performed to identify differentially expressed genes using SAS JMP10 Genomics, version 6, from SAS (SAS Institute, Cary, NC, USA). A false-positive rate of $a = 0.05$ with FDR correction was taken as the level of significance. Venn diagrams were created with the public available analysis tool of the Bioinformatic & Evolutionary Genomic server (http://bioinformatics.psb.ugent.be/webtools/Venn).

GSEA was performed by using the *fgsea* package (*52*) for R v3.4.0 (*53*). Pathways belonging to various cell functions were obtained from Kyoto Encyclopedia of Genes and Genomes (www.genome.jp/kegg).

Stable transformation of *A. thaliana* and selection of the transformed plants

Arabidopsis plants were stably transformed with the respective constructs by the established *A. tumefaciens*–mediated floral dip transformation method (*54*). Selection of 1-week-old soil-grown plants was performed by spraying glufosinate-ammonium solution (0.2 g/liter) three times within 6 days. The surviving plants were genotyped by PCR using specific primers (table S5).

Inhibition of proteasome with MG132 for the immunological detection of polyubiquitinated proteins

Leaf discs (five, diameter of 7 mm) of 6-week-old plants were floated on ½ Hoagland medium supplemented with 50 μM MG132 (Sigma-Aldrich) in the light at 22°C for 6 hours while shaking at 65 rpm. Excess liquid was removed, and the sample was immediately snap-frozen in liquid nitrogen. Leaf discs floated on ½ Hoagland served as a noninhibited proteasome control.

Quantification of plant proteins by immunological detection or nanoflow LC-MS^2 analysis

Proteins were extracted from *Arabidopsis* leaf or root tissue and separated by SDS-PAGE as described in (*55*). For immunological detection of polyubiquitinated proteins, SDS-PAGE–separated leaf proteins were blotted onto a polyvinylidene difluoride membrane that was blocked with 5% bovine serum albumin (BSA) in TBS-T [50 mM tris (pH 7.6), 150 mM NaCl, and 0.1% Tween 20] and subsequently decorated with the α-UBQ11 primary antibody (AS08307, Agrisera) diluted in 1:5000 in 0.5% BSA in TBS-T. The primary antibody was detected with goat anti-rabbit immunoglobulin G (H&L) horseradish peroxidase conjugate (AS09 602, Agrisera) diluted to 1:25,000 in 0.5% BSA in TBS-T. The horseradish peroxidase was visualized with the Pierce ECL Kit in combination with the Western Blotting Substrate (Thermo Fisher Scientific) according to the manufacturer's instructions. Signals were detected and quantified with the ImageQuant LAS 4000 controlled by the ImageQuant TL software (GE Healthcare).

High-performance LC–MS–based quantification of NatA subunits and HYPK

For MS-based quantification of NAA10, NAA15, and HYPK, individual proteins were manually excised from SDS-PAGE gels and processed as described with minor modifications (*56*). In brief, trypsin digestion was done overnight at 37°C. The reaction was quenched by the addition of 20 μl of 0.1% trifluoroacetic acid (TFA; Biosolve, Valkenswaard, Netherlands), and the supernatant was dried in a vacuum concentrator before LC-MS analysis. Nanoflow LC-MS^2 analysis was performed with an Ultimate 3000 LC system coupled to a Q Exactive HF mass spectrometer (Thermo Fisher Scientific, Bremen, Germany). Samples were dissolved in 0.1% TFA, injected to a self-packed analytical column (75 μm × 200 mm; ReproSil Pur 120 C18-AQ; Dr. Maisch GmbH), and eluted with solvent B [89.9% ACN (acetonitrile) (Biosolve) and 0.1% FA] with a flow rate of 300 nl min^{-1} in a linear gradient (acetonitrile gradient: 3 to 21.5%, 20 min; 21.5 to 35%, 4 min).

NAA15 was quantified from data acquired in a data-dependent acquisition mode, automatically switching between MS, acquired at 60,000 [mass/charge ratio (m/z) 400] resolution, and MS^2 spectra, generated for up to 15 precursors with normalized collision energy of 27%, measured at 15,000 resolution. To quantify NAA10, MS^2 spectra were acquired for up to nine unspecified precursors with additional five MS2 scans targeted for NAA10. Precursors for targeted analysis of NAA10 were m/z 538.2, 558.8, 743.3, 745.9, and 881.4. For HYPK, four additional MS2 scans were acquired in data-independent mode with m/z of 508.9, 596.3, 604.3, and 762.9.

To identify and quantify the proteins, raw files were analyzed using Proteome Discoverer with the Sequest (Thermo Fisher Scientific, San Jose, USA; version 2.2). Sequest was set up to search against *A. thaliana* databases (UP000006548_201709.fasta, 82,082 sequences and UP000006548 unreviewed_201709.fasta, 15,727 sequences), common contaminants (MaxQuant 1.5.3.30), and target proteins (NAA15, NAA10, and HYPK) with trypsin as the digestion enzyme. Parent ion mass tolerance was set to 10 parts per million (ppm), and fragment ion mass tolerance was set to 0.02 Da. Carbamidomethylation of cysteine was specified as a fixed modification. Oxidation of methionine and acetylation of the protein N terminus were specified as variable modifications. For MS1 quantification, protein abundances determined by Proteome Discoverer were used. NAA10 was quantified from MS2 scans using the most intense fragment of each peptide. Ratios were calculated from the averaged intensities from the different plant lines.

Quantification of proteasome activity in plants

Soluble proteins were extracted from leaf material, as stated above, with the exception that dithiothreitol and phenylmethylsulfonyl fluoride were avoided in the extraction buffer. The soluble proteins (0.1 mg) were dissolved in 100 mM tris-acetate buffer (pH 7) (0.89 ml) containing 25 μM proteasome substrate I (Z-Leu-Leu-Leu-AMC; Sigma-Aldrich) and incubated at 37°C for 45 min. The reaction was stopped by the addition of 0.1 ml of 10% SDS followed by dilution in 0.9 ml of 0.1 M tris-acetate buffer (pH 9). Fluorescence of the cleaved proteasome substrate I was detected at 440 nm with a FLUOstar OPTIMA plate reader (BMG Labtech) after specific excitation at 380 nm.

Determination of free N terminus levels

Soluble proteins were extracted from *Arabidopsis* leaves in citrate buffer [citric acid (0.172 g/liter), sodium citrate (14.41 g/liter), and

1 mM EDTA (pH 7)]. Free amino acids were removed with PD Spintrap G-25 columns (GE Healthcare). Protein (75 μg) was supplemented with citrate buffer and 500 μM NBD-Cl and incubated for 16 hours in the dark. The fluorescence intensity was measured in FLUOstar Omega plate reader (BMG Labtech) with Ex/Em spectra 470 to 10/520 nm.

Quantification of the N^{α}-terminal acetylome

Determination of the NTA yield of proteins was performed in leaves of 6-week-old soil-grown plants. The N-acetylome of the proteins was determined with the SILProNAQ approach (*32*) followed by the application of the EnCOUNTEer parsing tool (*33*).

Global proteomics for quantification of protein steady-state levels

The global proteomics approach has been performed as described in (*18*). In brief, proteins were extracted from leaves of 6-week-old soil grown plants according to the in-StageTip protocol (*57*) and analyzed on an EASY-nLC 1200 UPLC system (Thermo Fisher Scientific) that was coupled to a Q Exactive HFX Orbitrap instrument. The resulting MS raw files were analyzed using the MaxQuant software, version 1.6.1.13 (*58*), and peptide lists were searched against the species level UniProt FASTA database. A contaminant database generated by the Andromeda search engine (*59*) was configured with cysteine carbamidomethylation as a fixed modification and N-terminal acetylation and methionine oxidation as variable modifications. We set the FDR to 0.01 for protein and peptide levels with a minimum length of seven amino acids for peptides. The FDR was determined by searching a reverse database. Enzyme specificity was set as C-terminal to arginine and lysine as expected using trypsin and LysC as proteases. A maximum of two missed cleavages was allowed. Peptide identification was performed in Andromeda with an initial precursor mass deviation up to 7 ppm and a fragment mass deviation of 20 ppm. All proteins and peptides matching to the reversed database were filtered out. Bioinformatic analyses were performed using Perseus (*60*).

Quantification of global protein turnover by isotope labeling

The global protein turnover rates in leaves of approximately 6-week-old soil-grown plants were quantified by specific isotope labeling with the EasyTag EXPRESS^{35}S protein labeling mix (11 mCi/ml; PerkinElmer).

For determination of translation rates in planta, leaf discs (four, diameter of 7 mm) were floated on ½ Hoagland medium supplemented with 70 μCi/ml for up to 90 min. Samples were harvested at indicated time points, washed, and immediately snap-frozen in liquid nitrogen. The material was ground to a fine powder and extracted on ice with 0.3 ml of 50 mM Hepes, 10 mM KCl, 1 mM EDTA, 1 mM EGTA, and 10% (v/v) glycerine (pH 7.4) for 15 min. Samples were centrifuged (15,000*g*, 4°C, 15 min), and the supernatant was diluted in 0.3 ml of buffer. Excess Easy Tag label was removed from the sample (0.15 ml) with a PD Spintrap G-25 column (GE Healthcare). An aliquot (30 μl) of the purified protein sample was dissolved in 10 ml of liquid scintillation cocktail (Ultima Gold, PerkinElmer), and the protein-incorporated isotope label was quantified with the Tri-Carb 2810TR Liquid Scintillation Analyzer (PerkinElmer). The detected signal was normalized to the fresh weight of the sample after background subtraction.

To quantify the in vivo protein degradation rates, proteins were labeled by incubating leaf discs for 17.5 hours with ½ Hoagland medium supplemented with 88 μCi of EasyTag EXPRES ^{35}S-protein labeling. At time point zero, the leaf discs (four, diameter of 7 mm) were transferred to ½ Hoagland medium containing 1 mM cycloheximide for up to 6 hours. The cycloheximide containing solution was replaced every 60 min to ensure translation arrest. Samples were harvested at indicated time points, and the proteins were prepared as described above for quantification of protein-incorporated isotope label. The normalized signal intensity at time point zero was set to 100%.

Noninvasive relative protein lifetime measurements in plants

For quantification of the protein lifetime in planta with the tFT, we replaced the serine acetyltransferase 5 (SAT5) sequence in the previously described pBinAR::SAT5-tFT construct (*34*) with the orf encoding the protein of interest. The required endonuclease restriction sites were fused to these orfs by PCR amplification with specific primers (table S5). Transient transformation of *Arabidopsis* leaf cells, confocal microscopy, and evaluation of relative protein lifetime were performed as described previously (*34*).

Statistical analysis

The Holm-Sidak one-way ANOVA or the unpaired Student's *t* test of the SIGMA Plot12 software suite was applied for the detection of statistically significant differences between sample groups. Asterisks ($^{*}P \leq 0.05$, $^{**}P \leq 0.01$, $^{***}P \leq 0.001$) or letters indicate individual groups identified by the Student's *t* test or pairwise multiple comparisons with the Kruskal-Wallis or the Holm-Sidak one-way ANOVA, respectively.

SUPPLEMENTARY MATERIALS

Supplementary material for this article is available at https://science.org/doi/10.1126/sciadv.abn6153

View/request a protocol for this paper from *Bio-protocol*.

REFERENCES AND NOTES

1. T. Arnesen, P. van Damme, B. Polevoda, K. Helsens, R. Evjenth, N. Colaert, J. E. Varhaug, J. Vandekerckhove, J. R. Lillehaug, F. Sherman, K. Gevaert, Proteomics analyses reveal the evolutionary conservation and divergence of N-terminal acetyltransferases from yeast and humans. *Proc. Natl. Acad. Sci. U.S.A.* **106**, 8157–8162 (2009).
2. W. V. Bienvenut, D. Sumpton, A. Martinez, S. Lilla, C. Espagne, T. Meinnel, C. Giglione, Comparative large scale characterization of plant versus mammal proteins reveals similar and idiosyncratic N-α-acetylation features. *Mol. Cell. Proteomics* **11**, M111.015131 (2012).
3. C. Giglione, T. Meinnel, Evolution-driven versatility of N terminal acetylation in photoautotrophs. *Trends Plant Sci.* **26**, 375–339 (2021).
4. E. Linster, M. Wirtz, N-terminal acetylation: An essential protein modification emerges as an important regulator of stress responses. *J. Exp. Bot.* **69**, 4555–4568 (2018).
5. W. V. Bienvenut, A. Brünje, J. B. Boyer, J. S. Mühlenbeck, G. Bernal, I. Lassowskat, C. Dian, E. Linster, T. V. Dinh, M. M. Koskela, V. Jung, J. Seidel, L. K. Schyrba, A. Ivanauskaite, J. Eirich, R. Hell, D. Schwarzer, P. Mulo, M. Wirtz, T. Meinnel, C. Giglione, I. Finkemeier, Dual lysine and N-terminal acetyltransferases reveal the complexity underpinning protein acetylation. *Mol. Syst. Biol.* **16**, e9464 (2020).
6. T. V. Dinh, W. V. Bienvenut, E. Linster, A. Feldman-Salit, V. A. Jung, T. Meinnel, R. Hell, C. Giglione, M. Wirtz, Molecular identification and functional characterization of the first Nα-acetyltransferase in plastids by global acetylome profiling. *Proteomics* **15**, 2426–2435 (2015).
7. E. Linster, D. Layer, W. V. Bienvenut, T. V. Dinh, F. A. Weyer, W. Leemhuis, A. Brünje, M. Hoffrichter, P. Miklankova, J. Kopp, K. Lapouge, J. Sindlinger, D. Schwarzer, T. Meinnel, I. Finkemeier, C. Giglione, R. Hell, I. Sinning, M. Wirtz, The Arabidopsis Nα-acetyltransferase NAA60 locates to the plasma membrane and is vital for the high salt stress response. *New Phytol.* **228**, 554–569 (2020).

8. P. Pesaresi, N. A. Gardner, S. Masiero, A. Dietzmann, L. Eichacker, R. Wickner, F. Salamini, D. Leister, Cytoplasmic N-terminal protein acetylation is required for efficient photosynthesis in Arabidopsis. *Plant Cell* **15**, 1817–1832 (2003).
9. M. Huber, W. V. Bienvenut, E. Linster, I. Stephan, L. Armbruster, C. Sticht, D. Layer, K. Lapouge, T. Meinnel, I. Sinning, C. Giglione, R. Hell, M. Wirtz, NatB-mediated N-terminal acetylation affects growth and biotic stress responses. *Plant Physiol.* **182**, 792–806 (2020).
10. E. Linster, I. Stephan, W. V. Bienvenut, J. Maple-Grødem, L. M. Myklebust, M. Huber, M. Reichelt, C. Sticht, S. Geir Møller, T. Meinnel, T. Arnesen, C. Giglione, R. Hell, M. Wirtz, Downregulation of N-terminal acetylation triggers ABA-mediated drought responses in Arabidopsis. *Nat. Commun.* **6**, 7640 (2015).
11. S. Deng, R. Marmorstein, Protein N-terminal acetylation: Structural basis, mechanism, versatility, and regulation. *Trends Biochem. Sci.* **4**, 15–27 (2020).
12. L. Armbruster, E. Linster, J. B. Boyer, A. Brünje, J. Eirich, I. Stephan, W. V. Bienvenut, J. Weidenhausen, T. Meinnel, R. Hell, I. Sinning, I. Finkemeier, C. Giglione, M. Wirtz, NAA50 is an enzymatically active N^{α}-acetyltransferase that is crucial for development and regulation of stress responses. *Plant Physiol.* **183**, 1502–1516 (2020).
13. F. Xu, Y. Huang, L. Li, P. Gannon, E. Linster, M. Huber, P. Kapos, W. Bienvenut, B. Polevoda, T. Meinnel, R. Hell, C. Giglione, Y. Zhang, M. Wirtz, S. Chen, X. Li, Two N-terminal acetyltransferases antagonistically regulate the stability of a nod-like receptor in Arabidopsis. *Plant Cell* **27**, 1547–1562 (2015).
14. R. D. Vierstra, The ubiquitin-26S proteasome system at the nexus of plant biology. *Nat. Rev. Mol. Cell Biol.* **10**, 385–397 (2009).
15. H. Aksnes, R. Ree, T. Arnesen, Co-translational, post-translational, and non-catalytic roles of N-terminal acetyltransferases. *Mol. Cell* **73**, 1097–1114 (2019).
16. A. Shemorry, C. S. Hwang, A. Varshavsky, Control of protein quality and stoichiometries by N-terminal acetylation and the N-end rule pathway. *Mol. Cell* **50**, 540–551 (2013).
17. D. J. Gibbs, M. Bailey, H. M. Tedds, M. J. Holdsworth, From start to finish: Amino-terminal protein modifications as degradation signals in plants. *New Phytol.* **211**, 1188–1194 (2016).
18. E. Linster, F. L. Forero Ruiz, P. Miklankova, T. Ruppert, J. Mueller, L. Armbruster, X. Gong, G. Serino, M. Mann, R. Hell, M. Wirtz, Cotranslational N-degron masking by acetylation promotes proteome stability in plants. *Nat. Commun.* **13**, 810 (2022).
19. A. Martinez, J. A. Traverso, B. Valot, M. Ferro, C. Espagne, G. Ephritikhine, M. Zivy, C. Giglione, T. Meinnel, Extent of N-terminal modifications in cytosolic proteins from eukaryotes. *Proteomics* **8**, 2809–2831 (2008).
20. M. Gautschi, S. Just, A. Mun, S. Ross, P. Rücknagel, Y. Dubaquié, A. Ehrenhofer-Murray, S. Rospert, The yeast N^{α}-acetyltransferase NatA is quantitatively anchored to the ribosome and interacts with nascent polypeptides. *Mol. Cell. Biol.* **23**, 7403–7414 (2003).
21. R. S. Magin, S. Deng, H. Zhang, B. Cooperman, R. Marmorstein, Probing the interaction between NatA and the ribosome for co-translational protein acetylation. *PLOS ONE* **12**, e0186278 (2017).
22. T. Arnesen, D. Anderson, J. Torsvik, H. B. Halseth, J. E. Varhaug, J. R. Lillehaug, Cloning and characterization of hNAT5/hSAN: An evolutionarily conserved component of the NatA protein N-alpha-acetyltransferase complex. *Gene* **371**, 291–295 (2006).
23. F. Hou, C. W. Chu, X. Kong, K. Yokomori, H. Zou, The acetyltransferase activity of San stabilizes the mitotic cohesin at the centromeres in a shugoshin-independent manner. *J. Cell Biol.* **177**, 587–597 (2007).
24. M. Neubauer, R. W. Innes, Loss of the acetyltransferase NAA50 induces endoplasmic reticulum stress and immune responses and suppresses growth. *Plant Physiol.* **183**, 1838–1854 (2020).
25. J. Weidenhausen, J. Kopp, L. Armbruster, M. Wirtz, K. Lapouge, I. Sinning, Structural and functional characterization of the N-terminal acetyltransferase NAA50. *Structure* **29**, 413–425.e5 (2021).
26. P. W. Faber, G. T. Barnes, J. Srinidhi, J. Chen, J. F. Gusella, M. MacDonald, Huntingtin interacts with a family of WW domain proteins. *Hum. Mol. Genet.* **7**, 1463–1474 (1998).
27. S. Deng, N. McTiernan, X. Wei, T. Arnesen, R. Marmorstein, Molecular basis for N-terminal acetylation by human NatE and its modulation by HYPK. *Nat. Commun.* **11**, 818 (2020).
28. F. A. Weyer, A. Gumiero, K. Lapouge, G. Bange, J. Kopp, I. Sinning, Structural basis of HypK regulating N-terminal acetylation by the NatA complex. *Nat. Commun.* **8**, 15726 (2017).
29. L. Gottlieb, R. Marmorstein, Structure of human NatA and its regulation by the huntingtin interacting protein HYPK. *Structure* **26**, 925–935.e8 (2018).
30. T. Arnesen, K. K. Starheim, P. van Damme, R. Evjenth, H. Dinh, M. J. Betts, A. Ryningen, J.. Vandekerckhove, K. Gevaert, D. Anderson, The chaperone-like protein HYPK acts together with NatA in cotranslational N-terminal acetylation and prevention of Huntingtin aggregation. *Mol. Cell. Biol.* **30**, 1898–1909 (2010).
31. H. Chen, Y. Zou, Y. Shang, H. Lin, Y. Wang, R. Cai, X. Tang, J. M. Zhou, Firefly luciferase complementation imaging assay for protein-protein interactions in plants. *Plant Physiol.* **146**, 368–376 (2008).
32. W. V. Bienvenut, C. Giglione, T. Meinnel, SILProNAQ: A convenient approach for proteome-wide analysis of protein N-termini and N-terminal acetylation quantitation. *Methods Mol. Biol.* **1574**, 17–34 (2017).
33. W. V. Bienvenut, J. P. Scarpelli, J. Dumestier, T. Meinnel, C. Giglione, EnCOUNTer: A parsing tool to uncover the mature N-terminus of organelle-targeted proteins in complex samples. *BMC Bioinformatics* **18**, 182 (2017).
34. H. Zhang, E. Linster, L. Gannon, W. Leemhuis, C. A. Rundle, F. L. Theodoulou, M. Wirtz, Tandem fluorescent protein timers for noninvasive relative protein lifetime measurement in plants. *Plant Physiol.* **180**, 718–731 (2019).
35. R. Ree, S. Varland, T. Arnesen, Spotlight on protein N-terminal acetylation. *Exp. Mol. Med.* **50**, 1–13 (2018).
36. G. Kramer, D. Boehringer, N. Ban, B. Bukau, The ribosome as a platform for co-translational processing, folding and targeting of newly synthesized proteins. *Nat. Struct. Mol. Biol.* **16**, 589–597 (2009).
37. S. Raychaudhuri, M. Sinha, D. Mukhopadhyay, N. P. Bhattacharyya, HYPK, a Huntingtin interacting protein, reduces aggregates and apoptosis induced by N-terminal Huntingtin with 40 glutamines in Neuro2a cells and exhibits chaperone-like activity. *Hum. Mol. Genet.* **17**, 240–255 (2008).
38. S. Raychaudhuri, R. Banerjee, S. Mukhopadhyay, N. P. Bhattacharyya, Conserved C-terminal nascent peptide binding domain of HYPK facilitates its chaperone-like activity. *J. Biosci.* **39**, 659–672 (2014).
39. W. M. Holmes, B. K. Mannakee, R. N. Gutenkunst, T. R. Serio, Loss of amino-terminal acetylation suppresses a prion phenotype by modulating global protein folding. *Nat. Commun.* **5**, 4383 (2014).
40. T. Hander, Á. D. Fernández-Fernández, R. P. Kumpf, P. Willems, H. Schatowitz, D. Rombaut, A. Staes, J. Nolf, R. Pottie, P. Yao, A. Gonçalves, B. Pavie, T. Boller, K. Gevaert, F. Van Breusegem, S. Bartels, S. Stael, Damage on plants activates Ca^{2+}–dependent metacaspases for release of immunomodulatory peptides. *Science* **363**, eaar7486 (2019).
41. D. K. Ghosh, A. Roy, A. Ranjan, Aggregation-prone regions in HYPK help it to form sequestration complex for toxic protein aggregates. *J. Mol. Biol.* **430**, 963–986 (2018).
42. G. Liszczak, J. M. Goldberg, H. Foyn, E. J. Petersson, T. Arnesen, R. Marmorstein, Molecular basis for N-terminal acetylation by the heterodimeric NatA complex. *Nat. Struct. Mol. Biol.* **20**, 1098–1105 (2013).
43. D. Gawron, E. Ndah, K. Gevaert, P. Van Damme, Positional proteomics reveals differences in N-terminal proteoform stability. *Mol. Syst. Biol.* **12**, 858 (2016).
44. C. H. Yi, H. Pan, J. Seebacher, I. H. Jang, S. G. Hyberts, G. J. Heffron, M. G. Vander Heiden, R. Yang, F. Li, J. W. Locasale, H. Sharfi, B. Zhai, R. Rodriguez-Mias, H. Luithardt, L. C. Cantley, G. Q. Daley, J. M. Asara, S. P. Gygi, G. Wagner, C. F. Liu, J. Yuan, Metabolic regulation of protein N-alpha-acetylation by Bcl-xL promotes cell survival. *Cell* **146**, 607–620 (2011).
45. R. T. Timms, Z. Zhang, D. Y. Rhee, J. W. Harper, I. Koren, S. J. Elledge, A glycine-specific N-degron pathway mediates the quality control of protein *N*-myristoylation. *Science* **365**, eaaw4912 (2019).
46. F. Mueller, A. Friese, C. Pathe, R. Cardoso da Silva, K. B. Rodriguez, A. Musacchio, T. Bange, Overlap of NatA and IAP substrates implicates N-terminal acetylation in protein stabilization. *Sci. Adv.* **7**, eabc8590 (2021).
47. L. M. Myklebust, P. van Damme, S. I. Støve, M. J. Dörfel, A. Abboud, T. V. Kalvik, C. Grauffel, V. Jonckheere, Y. Wu, J. Swensen, H. Kaasa, G. Liszczak, R. Marmorstein, N. Reuter, G. J. Lyon, K. Gevaert, T. Arnesen, Biochemical and cellular analysis of Ogden syndrome reveals downstream Nt-acetylation defects. *Hum. Mol. Genet.* **24**, 1956–1976 (2015).
48. P. Tocquin, L. Corbesier, A. Havelange, A. Pieltain, E. Kurtem, G. Bernier, C. Périlleux, A novel high efficiency, low maintenance, hydroponic system for synchronous growth and flowering of *Arabidopsis thaliana*. *BMC Plant Biol.* **3**, 2 (2003).
49. K. Edwards, C. Johnstone, C. Thompson, A simple and rapid method for the preparation of plant genomic DNA for PCR analysis. *Nucleic Acids Res.* **19**, 1349 (1991).
50. L. Kong, J. Cheng, Y. Zhu, Y. Ding, J. Meng, Z. Chen, Q. Xie, Y. Guo, J. Li, S. Yang, Z. Gong, Degradation of the ABA co-receptor ABI1 by PUB12/13 U-box E3 ligases. *Nat. Commun.* **6**, 8630–8630 (2015).
51. M. Dai, P. Wang, A. D. Boyd, G. Kostov, B. Athey, E. G. Jones, W. E. Bunney, R. M. Myers, T. P. Speed, H. Akil, S. J. Watson, F. Meng, Evolving gene/transcript definitions significantly alter the interpretation of GeneChip data. *Nucleic Acids Res.* **33**, e175 (2005).
52. A. A. Sergushichev, An algorithm for fast preranked gene set enrichment analysis using cumulative statistic calculation. *bioRxiv* , 060012 (2016).
53. R Core Team, The R Project for Statistical Computing (2014); www.R-project.org/.
54. S. J. Clough, A. F. Bent, Floral dip: A simplified method for Agrobacterium-mediated transformation of *Arabidopsis thaliana*. *Plant J.* **16**, 735–743 (1998).
55. M. Wirtz, R. Hell, Dominant-negative modification reveals the regulatory function of the multimeric cysteine synthase protein complex in transgenic tobacco. *Plant Cell* **19**, 625–639 (2007).

56. C. Fecher-Trost, U. Wissenbach, A. Beck, P. Schalkowsky, C. Stoerger, J. Doerr, A. Dembek, M. Simon-Thomas, A. Weber, P. Wollenberg, T. Ruppert, R. Middendorff, H. H. Maurer, V. Flockerzi, The in vivo TRPV6 protein starts at a non-AUG triplet, decoded as methionine, upstream of canonical initiation at AUG. *J. Biol. Chem.* **288**, 16629–16644 (2013).
57. N. A. Kulak, G. Pichler, I. Paron, N. Nagaraj, M. Mann, Minimal, encapsulated proteomic-sample processing applied to copy-number estimation in eukaryotic cells. *Nat. Methods* **11**, 319–324 (2014).
58. J. Cox, M. Mann, MaxQuant enables high peptide identification rates, individualized p.p.b.-range mass accuracies and proteome-wide protein quantification. *Nat. Biotechnol.* **26**, 1367–1372 (2008).
59. J. Cox, N. Neuhauser, A. Michalski, R. A. Scheltema, J. V. Olsen, M. Mann, Andromeda: A peptide search engine integrated into the MaxQuant environment. *J. Proteome Res.* **10**, 1794–1805 (2011).
60. S. Tyanova, T. Temu, P. Sinitcyn, A. Carlson, M. Y. Hein, T. Geiger, M. Mann, J. Cox, The Perseus computational platform for comprehensive analysis of (prote)omics data. *Nat. Methods* **13**, 731–740 (2016).

Acknowledgments: We are grateful for the excellent technical and scientific support on confocal laser scanning microscopy by the Nikon Imaging Center (NIC; COS Heidelberg) and on MS-based identification and quantification of proteins by the Core Facility for Mass Spectrometry & Proteomics (CFMP, ZMBH Heidelberg). We are indebted to O. Keberlein for excellent technical support and V. Braun for help with the characterization of the growth phenotypes of the mutants. We thank G. Stier for providing vectors, F. Weyer for plasmids (pET24d::*Ct*Naa10-His_6 and pET24d::*Ct*Naa15) and for human and *Chaetomium* cDNA, and S. A. and S. Jaeger for cloning. Project IDs 201348542 and 496871662. **Funding:** Research at Heidelberg University was funded by the Deutsche Forschungsgemeinschaft (DFG, German Research Foundation), Project-IDs 201348542 and SFB 1036, research grant (WI 3560/4-1 and WI 3560/7-1), and via the Leibniz Programme (DFG-IS-586/6-1) to I.S. We are grateful for the support of P.M., E.L., J.W., and L.A. by the Heidelberg Biosciences International Graduate School (HBIGS). Research at the University Paris-Saclay was funded by the French Agence Nationale de la Recherche (ANR-13-BSV6-0004 and ANR-17-CAPS-0001-01) and benefits from the support of the Labex Saclay Plant Sciences SPS (ANR-10-LABX-0040-SPS) and from the facilities and expertise of the I2BC proteomic platform SICaPS, supported by IBiSA, Ile de France Region, Plan Cancer, CNRS, and Paris-Saclay University. **Author contributions:** P.M. performed phenotypic analysis and analyzed the drought stress response of *hypk* plants; performed complementation studies of *hypk-3* with *Hs*HYPK and *Ct*HYPK and analyzed the transgenic plants, detected level of polyubiquitinylated proteins, and proteasome activity; and performed translation and degradation assay, genotyping, and qRT-PCR analysis. E.L. designed and performed in vivo determination of protein half-life times. L.A. designed and performed luciferase assay. W.B. participated in the initial N-terminomic data acquisition. J.-B.B., C.G., and T.M. designed, performed, and analyzed N-terminomic data. J.W., K.L., and I.S. produced proteins and designed and performed protein-protein interaction studies of *At*HYPK with *Ct*NatA, or *At*NAA15. C.S. and C.D.L.T. performed transcriptome analysis and evaluated the data. J.M. and M.M. quantified and analyzed steady-state protein levels in wild type and *hypk* lines by LC-MS^2. C.G. and I.S. acquired funding and contributed to manuscript writing. R.H. and M.W. designed the study and wrote the manuscript. **Competing interests:** The authors declare that they have no competing interests. **Data and materials availability:** MS-based proteomics data for determination of the N-terminal acetylation status (N-acetylome), the abundance of HYPK and NatA subunits, and the steady-state levels of leaf proteins in the wild type and hypk lines are deposited in the ProteomeXchange Consortium (http://proteomecentral.proteomexchange.org/cgi/GetDataset) via the PRIDE repository (www.ebi.ac.uk/pride/) with the dataset identifiers PXD023195, PXD023599, and PXD022120, respectively. The transcriptome data are deposited in the Gene Expression Omnibus public data repository (www.ncbi.nlm.nih.gov/geo/) under the accession number: GSE158586. All T-DNA insertion plant lines used in this study can be obtained from Nottingham Arabidopsis Stock Centre (NASC; https://arabidopsis.info/BasicForm).

Submitted 9 December 2021
Accepted 29 April 2022
Published 15 June 2022
10.1126/sciadv.abn6153

ScienceAdvances

HYPK promotes the activity of the *N*-acetyltransferase A complex to determine proteostasis of nonAc-X/N-degron–containing proteins

Pavlína MiklánkováEric LinsterJean-Baptiste BoyerJonas WeidenhausenJohannes MuellerLaura ArmbrusterKarine LapougeCarolina De La TorreWilly BienvenutCarsten StichtMatthias MannThierry MeinnelIrmgard SinningCarmela GiglioneRüdiger HellMarkus Wirtz

Sci. Adv., 8 (24), eabn6153. • DOI: 10.1126/sciadv.abn6153

Science Advances (ISSN) is published by the American Association for the Advancement of Science. 1200 New York Avenue NW, Washington, DC 20005. The title *Science Advances* is a registered trademark of AAAS.